Molecular Dynamics Modeling of Ion Adsorption to the Basal Surfaces of Kaolinite

Igor F. Vasconcelos* and Bruce A. Bunker

Department of Physics, University of Notre Dame, Notre Dame, Indiana 46556

Randall T. Cygan

Geochemistry Department, Sandia National Laboratories, Albuquerque, New Mexico 87185-0754

Received: September 1, 2006; In Final Form: March 5, 2007

Molecular dynamics simulation is used to study the mechanisms involved in the adsorption of various ions to the basal surfaces of kaolinite. Analysis of simulation data indicates that cations and anions adsorb preferably on the siloxane and gibbsite surfaces of kaolinite, respectively. Strong inner-sphere adsorption of chlorine at aluminum vacancies on the gibbsite surface and the occurrence of chlorine-driven inner-sphere adsorption of cesium and sodium on the gibbsite surface for high ionic strengths are observed. Cesium ions form strong inner-sphere complexes at ditrigonal cavities on the siloxane surface. Outer-sphere cesium is highly mobile and only weak adsorption may occur. A small amount of sodium adsorbs on the siloxane surface as inner-sphere complexes at less clearly defined sites. Like cesium, sodium only forms very weak outer-sphere complexes on this surface. Inner-sphere complexes of cadmium and lead do not occur on either surface. Relatively strong outer-sphere cadmium and lead complexes are present on the siloxane surface at ditrigonal cavities.

1. Introduction

The fate of chemical and radioactive wastes, such as radionuclides and heavy metals, in the environment is controlled, to an extended degree, by the ability of subsurface minerals to uptake these contaminants by processes like permanent adsorption and precipitation. Clay minerals are of critical importance for these processes. Because of their relatively large surface area and surface reactivity, clays are often able to regulate the composition of soil by adsorbing metals, protons, and organic molecules. They also play an important role in the transport of sorbed contaminants in groundwater.

Clay minerals are abundant in many near-surface geological environments and are highly sorptive due to their small particle sizes, large surface areas, and chemically active surface defect sites. Recognition of the significance of these minerals has recently increased because of the need for environmental remediation. For instance, the reaction of metal cations with mineral surfaces in and near hazardous chemical and radioactive waste sites often controls the fates of these species.

Kaolinite[1,2,3,4] ($Al_2Si_2O_5(OH)_4$) is a 1:1 layer clay composed of a repeating layer of a gibbsite aluminum octahedral sheet and a siloxane silicon tetrahedral sheet. Octahedral and tetrahedral sheets are connected together by bridging oxygens. Each silicon is connected to three other silicon atoms by bridging oxygens forming the siloxane surface. This arrangement of tetrahedral silicons gives rise to hexagonal cavities on the surface. In the gibbsite sheet, each aluminum is coordinated by two oxygens of the siloxane sheet and shares four hydroxyls with neighboring aluminum atoms. Three of these hydroxyls are oriented toward the external surface forming the gibbsite surface while the fourth one is oriented inward in the direction of the siloxane cavity.[5] This layered structure extends to edges of the crystal where exposed dangling silicon and aluminum atoms are terminated by hydroxyls at low pH conditions.

The ion retention capabilities of kaolinite are known to be low with respect to smectites and illites and most of the long-term adsorption is due to the presence of impurities.[6] However, kaolinite is of interest because many nuclear and nuclear waste sites are located on kaolinite-rich soils where even limited retention capacity would be important in the migration of contaminants over distances measured in kilometers. Furthermore, kaolinite provides a relatively simple substrate for studying surface adsorption due to its lack of interlayer metal sites and the presence of both hydrophilic and hydrophobic basal surfaces, which makes it an attractive model phase of study.

Adsorption on clay minerals can occur via two mechanisms: outer-sphere adsorption, which often occurs on the basal planes existing on the external surfaces and interlayer regions of clays minerals, and inner-sphere adsorption, which occurs mostly at the silicon hydroxyls (silanols) and aluminum hydroxyls (aluminols) existing on the edge of clay minerals.[7,8] It is known that the adsorption mechanisms are different for various metal cations and therefore individual studies are required.

This paper presents studies on the structure and dynamics of adsorbed Cs^+, Na^+, Cd^{2+}, and Pb^{2+} in the mineral/aqueous solution interface at the basal surfaces of kaolinite. Cesium, cadmium, and lead are of great interest in environmental science applications due to their toxic nature. Sodium, on the other hand, is a very common ion in background electrolytes and hence it is important to understand its role in adsorption processes.

Cadmium and lead are highly toxic elements that can pollute water and soils due to their numerous industrial uses. Adsorption of cadmium and lead onto clay particles largely determines their availability within the environment and it has been the subject of many studies over the years (cadmium[8−13] and lead[9,14−16]).

The interaction between cadmium and lead and kaolinite surfaces can be summarized as follows: adsorption isotherms[17]

* Address correspondence to this author. E-mail: ifvasco@ufc.br.

10.1021/jp065687+ CCC: $37.00
Published on Web 04/14/2007

TABLE 1: Nonbond Parameters for the CLAYFF Force Field[a] [Reference 5]

force field type	symbol	charge (e)	ϵ (kcal/mol)	σ (Å)
water hydrogen	h*	0.410		
water oxygen	o*	−0.820	0.1554	3.1655
hydroxyl hydrogen	ho	0.425		
hydroxyl oxygen	oh	−0.950	0.1554	3.1655
bridging oxygen	ob	−1.050	0.1554	3.1655
tetrahedral silicon	st	2.100	1.8405×10^{-6}	3.3020
octahedral aluminum	ao	1.575	1.3298×10^{-6}	4.2713
aqueous chlorine ion	Cl	−1.000	0.1001	4.4000
aqueous cesium ion	Cs	1.000	0.1000	3.8310
aqueous sodium ion	Na	1.000	0.1301	2.3500
aqueous cadmium ion	Cd	2.000	0.0470	2.7628
aqueous lead ion	Pb	2.000	0.1182	3.3243

[a] The parameters ϵ and σ determine Lennard-Jones potential well depth and equilibrium distance, respectively.

indicate that cadmium adsorbs very little to kaolinite at pH <7. At pH 8, adsorption began to increase rapidly and at pH 9 most of the cadmium is adsorbed to the kaolinite surface. Adsorption isotherms also indicate a small percentage of lead adsorbed to kaolinite between pH 4.5 and 6. At pH >6, adsorption begins to increase until pH 8 at which point most of the lead is adsorbed to the kaolinite surface. The low adsorption in acidic conditions can be explained by the competition between protons and metallic cations for the edge aluminols and silanols leaving the basal surfaces as the primary destination for the cations.

^{137}Cs is an important component of nuclear waste and its storage and migration in natural environments have been studied by many investigators.[18−26] ^{137}Cs has been introduced to soils and groundwater over the past five decades by nuclear accidents, as fallout from nuclear testing, and as a byproduct of nuclear research and weapons production. Measurements of relative adsorption as a function of pH (adsorption isotherms)[20] suggest a pH dependent affinity of Cs^+ for the Al octahedral edge sites of the crystal and only a possible weak binding on the tetrahedral Si edge site at high pH values. Adsorption on the basal surfaces appears to be pH independent. There appears to be a significant pH independent amount of adsorption indicating a stronger interaction of cesium with the basal surfaces of kaolinite as opposed to cadmium and lead.

2. The Model

The CLAYFF force field[5] was used to model kaolinite and its interface aqueous solutions of CsCl, NaCl, $CdCl_2$, and $PbCl_2$. CLAYFF has been used successfully to obtain structural and dynamical properties of hydrated mineral systems and their interfaces with aqueous solutions.[27,28] One of the key features of CLAYFF is its flexibility within the clay lattice where the metal−oxygen interactions are described by a 12−6 Lennard-Jones term and a Coulombic function with partial charges derived by quantum chemistry methods.[29] The only bonded interactions are those within water molecules (bond stretch and angle bend) and hydroxyls (bond stretch) based on the SPC water model,[30] which has been used to study properties of bulk water and aqueous systems.[30−33] The SPC water model is relatively simple and has partial charges centered directly on each of the three atoms. Tables 1 and 2 show the force field parameters for all nonbonded and bonded interactions, respectively.

Kaolinite ($Al_2Si_2O_5(OH)_4$) is a 1:1 layer clay composed of a layer made up of a AlO_6 octahedral sheet and a SiO_4 tetrahedral sheet. Layers are kept together by hydrogen bonds between hydroxyl groups extending from the octahedral surface of a layer

TABLE 2: Bond Parameters for the CLAYFF Force Field

Bond Stretch			
species *i*	species *j*	k_b (kcal/mol Å^2)	r_o (Å)
o*	h*	554.1349	1.00
oh	ho	554.1349	1.00

Angle Bend				
species *i*	species *j*	species *k*	k_a (kcal/mol rad^2)	θ_o (deg)
h*	o*	h*	45.7696	109.47

to the basal oxygens on the tetrahedral surface of the next layer. For the present work, equilibrated, neutral kaolinite structures as those obtained in ref 5 are used. They were converted into orthogonal cells oriented in a such way that the (001) and (00$\bar{1}$) planes correspond to the octahedral and tetrahedral basal surfaces, respectively.

The simulation cells contain 243 kaolinite unit cells ($9 \times 9 \times 3$ units in the *a*, *b*, and *c* dimensions) with a total of 8262 atoms in the solid. The corresponding *a* and *b* dimensions are 46.5 and 80.3 Å and are fixed over all the simulations. The kaolinite crystal and solution are charge neutral, making our results pH independent. The basal surface of kaolinite controls adsorption at lower pH values, while at higher pH values the edge sites are expected to be dominant.

To simulate the solid/liquid interface, an aqueous region of dimensions 46.5 Å × 80.3 Å × 35.4 Å with 3600 water molecules is brought in contact with one of the basal surfaces of kaolinite to create the initial crystal−aqueous solution cell with a *c* dimension of 57.1 Å. We impose periodic boundary conditions on the three dimensions so that both basal surfaces are in contact with the solution, and run short NPT simulations (with only the *c* dimension allowed to vary) to equilibrate the solid/liquid interfaces. Kaolinite is a unique mineral because both (001) and (00$\bar{1}$) surfaces are exposed to the aqueous solution and molecular dynamics simulations provide an opportunity to examine both surfaces simultaneously, and that direct comparisons can be made from results.

Finally, 7, 32, and 64 cations (and the required number of Cl^- anions to ensure charge neutrality) are inserted in the solution to create 0.1, 0.5, and 1.0 M solutions for each of the four cations studied. The ions are randomly inserted just a few angstroms from the midplane of the aqueous region to avoid biased adsorption. After that, a few picoseconds of NPT dynamics is run to equilibrate the water structure around the added ions.

Materials Studio software (Accelrys, Inc., San Diego, CA) was used to create the simulation cells and to visualize the results and the LAMMPS (Large-scale Atomic/Molecular Massively Parallel Simulator) program[34] on a parallel Linux cluster to run all the simulations. The ensembles implemented are the constant NPT[35,36] (number of atoms, pressure 0 atm, and temperature 300 K) with only the *c* dimension allowed to vary and constant NVT[37,38] (number of atoms, volume, and temperature 300 K) with barostat and thermostat relaxation times of 100 and 500 fs, respectively. The equations of motion were integrated by using Verlet's algorithm[39,40] with time steps of 1 fs. We use the Ewald summation method[41] to calculate long-range electrostatic interactions.

A total of 12 (4 cations and 3 concentrations) of the optimized structures described above (a typical structure is shown in Figure1a) containing about 19000 atoms each as starting configurations are used for the molecular dynamics simulations

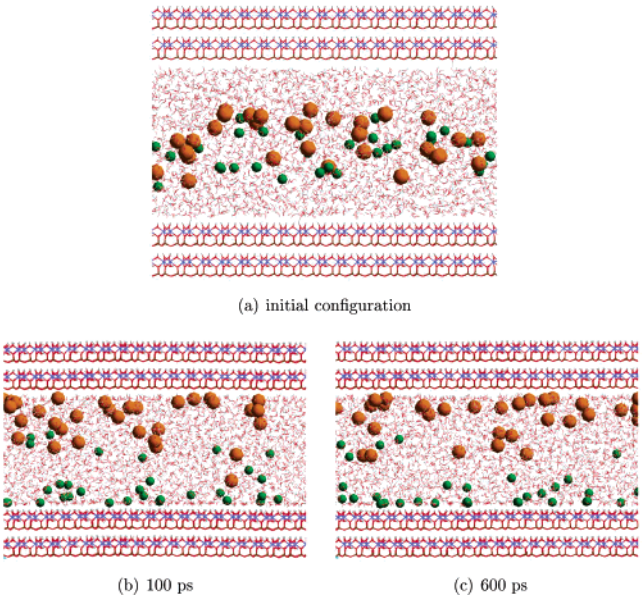

Figure 1. Equilibration of a 0.5 M CsCl system: (a) Graphical representation of the initial configuration of the 0.5 M CsCl solution in contact with the basal surfaces of kaolinite; (b) most of the adsorption has already occurred after 100 ps of dynamics; and (c) an extra 500 ps to ensure equilibration is run. Top and bottom surfaces are the tetrahedral SiO_4 and octahedral AlO_6 surfaces, respectively. Green and orange balls represent Cl^- and Cs^+ ions, respectively.

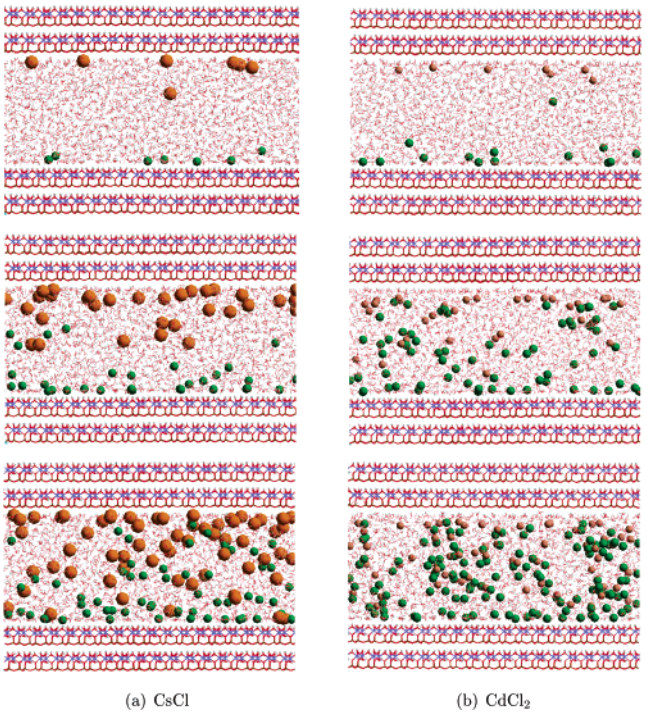

Figure 2. Configurations of each of the three concentrations of CsCl and $CdCl_2$ (0.1, 0.5, and 1.0 M from top to bottom) solutions in equilibrium with the basal surfaces of kaolinite.

presented in this study. In a typical complete simulation, the *c* dimension is first allowed to relax for a period of 100 ps of NPT dynamics. To ensure equilibrium of the adsorption dynamics, an extra NVT period of 500 ps is allowed. Equilibrium dynamic trajectories are finally recorded for each model for statistical analysis at 100 fs intervals during the next 500 ps of NVT dynamics to provide 5000 trajectory frames.

To analyze the results obtained from the various simulations, we calculate radial distribution functions[42] and atomic density profiles[27,28] in the [001] direction perpendicular to the solid/liquid interface (*c* dimension). Atomic density maps[27] are also calculated within planes parallel to the solid/liquid interfaces at characteristic distances to the surfaces for each atomic type involved in the adsorption processes.

3. Results and Discussions

Figure 1a shows the initial configuration of a 0.5 M CsCl solution in contact with the basal surfaces of kaolinite. A typical simulation starts from a structure similar to this. After just a few picoseconds, cations and anions diffuse preferentially toward the SiO_4 tetrahedral and AlO_6 octahedral surfaces, respectively. It can also be observed that the *c* dimension of the cell does not change during the last 50 ps indicating that the volume of the solution reached an equilibrium value.

Parts b and c of Figure 1 show graphical representations of the 0.5 M CsCl simulation cell after 100 and 600 ps of dynamics. A similar distribution of ions along the *c* axis can be seen in both structures, indicating that equilibrium is reached within that initial period of 100 ps. Stabilization of potential energy values (not shown) confirms equilibration after the 600 ps period. The pattern observed for other concentrations and other cations is consistent with this picture.

To investigate the adsorption processes as a function of ion loading, three concentrations (0.1, 0.5, and 1.0 M) of CsCl, NaCl, $CdCl_2$, and $PbCl_2$ are implemented. Figure 2 shows 0.1, 0.5, and 1.0 M CsCl and $CdCl_2$ solutions in equilibrium with the basal surfaces of kaolinite, after 600 ps. At lower ionic strengths (0.1 M), the solutions are far from saturation and there is a complete separation between cations and anions with virtually all ions associated with either surface (Figure 2, top two pictures). Cs^+ ions lose part of their hydration shell to come very close to the surface in an inner-sphere-like adsorption, while the presence of a layer of water between Cd^{2+} ions and the surface suggests that Cd^{2+} ions retain the structure of their bulk solution hydration shells forming what looks like outer-sphere adsorption complexes. It suggests strong and weak affinity between Cs^+ and Cd^{2+}, respectively, and the mineral surfaces. We will discuss these issues in detail later on. It is important to point out the contrast in water disposition immediately at the interfaces. The siloxane is relatively hydrophobic while the gibbsite surface (and hydroxyls) is hydrophilic and has significant hydrogen bonding. The flexible and unconstrained CLAYFF accurately models this type of behavior.

With increase in ionic strength, and consequent approach of saturation, there is an increasing number of ions remaining in the bulk solution. At 1.0 M, most of the ions are found in the bulk solution (Figure 2, bottom two pictures, and Figure 3) forming a structure similar to the original solution. Also at 1.0 M, the presence of some Cs^+ and Na^+ ions close to the AlO_6 octahedral surface could be noticed. Most of these ions are paired with a Cl^- ion suggesting a Cl^- driven adsorption of Cs^+ and Na^+ on the octahedral basal surface. The same, however, does not happen with Cd^{2+} and Pb^{2+} ions.

Before proceeding with further discussion, a definition of inner-sphere and outer-sphere adsorption in the scope of this work is required. An ion forms an inner-sphere adsorption complex if it is found, in equilibrium, at a distance of ~2.5−3.0 Å from a surface, with no water molecules between the metal and the surface, and has little mobility in the plane parallel to the surface, for a long enough period of simulation (500 ps). The same applies for the outer sphere, except the distances are ~2.0−2.5 Å beyond those of inner spheres. Outer-sphere

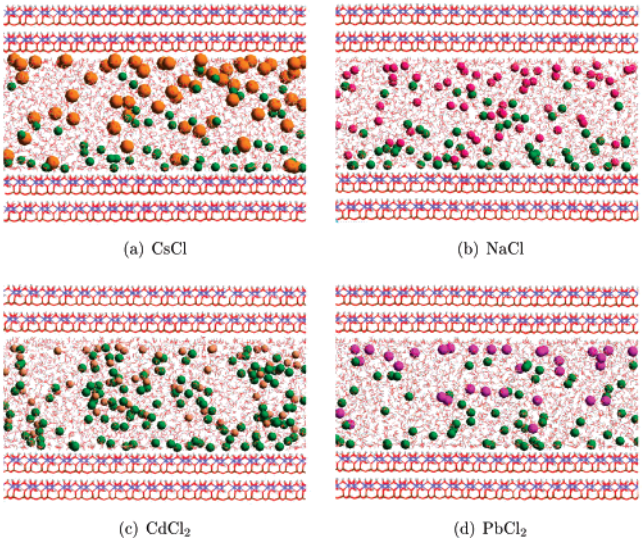

Figure 3. Representative configuration of equilibrated 1.0 M solutions in contact with the basal surfaces of kaolinites.

adsorption is also characterized by the presence of an intermediate water molecule between the metal and the surface.

Looking at the configurations of 1.0 M CsCl, NaCl, $CdCl_2$, and $PbCl_2$ solutions in equilibrium with kaolinite in Figure 3, some inferences can be made with respect to the adsorption processes. Adsorption mechanisms on the AlO_6 octahedral surface are mostly unchanged for the various cations and concentrations (except for the little Cl^- driven adsorption of Cs^+ and Na^+) and therefore will not be the focus of our discussion.

It is found that like Cd^{2+}, Pb^{2+} forms complexes consistent with outer-sphere adsorption on the tetrahedral SiO_4 surface. So does Na^+ with the exception of a few ions found at distances to the surface consistent with inner-sphere adsorption. However, as we will see later on, Na^+ ions have great mobility parallel to the mineral surface and fall outside our definition of adsorption. Cs^+ appears to adsorb as outer-sphere complexes as well but, very much like Na^+, these are very short-lived complexes and could hardly be regarded as adsorbed.

It has been so far assumed that the configurations shown in the previous figures are representative of the steady-state equilibrium of the mineral−solution interfaces. To validate (or negate) assumptions made above, it is necessary to extend the analysis beyond what can be inferred from assumed representative configurations. Atomic density profiles and atomic trajectory maps are used to achieve this goal.

3.1. Atomic Density Profiles. An atomic density profile[27,28] $\rho_i(z)$ is a measure of the probability of finding an atom of type i along the c axis, at distance z from a fixed origin. Density profiles are calculated by averaging the trajectories of each atomic species during 500 ps following the equilibration period. The integral of $\rho_i(z)$ over a certain range Δz gives the total number of species i atoms in the slab of area $a \times b$ and thickness Δz. Density profiles are a very effective tool to describe interfaces.

Figure 4 shows atomic density profiles for the three concentrations of CsCl solution in equilibrium with kaolinite. Regions 1 and 2 in the picture correspond to our definition of inner- and outer-sphere ranges given above. Water molecules in regions 1 at both surfaces form hydrogen bonds with oxygen/hydrogen atoms on either surface and are therefore strongly oriented. The presence of the surfaces affects the orientation of water molecules up to about 10 Å from either surface, from which

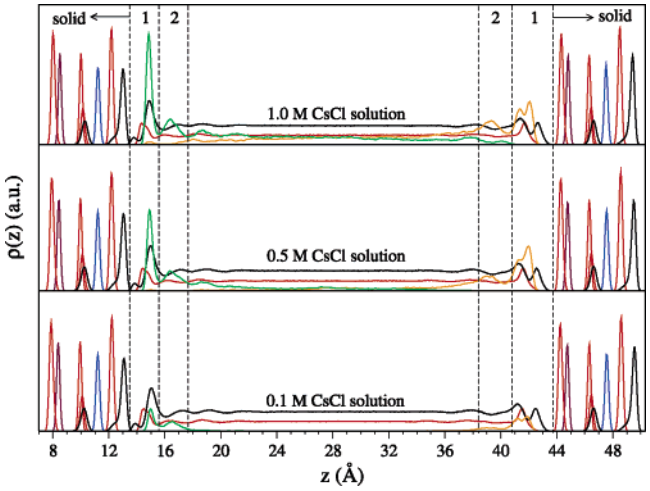

Figure 4. Atomic density profiles of the equilibrated 0.1, 0.5, and 1.0 M CsCl solutions in contact with the two basal surfaces of kaolinite. Color key: red (O), black (H), blue (Al), maroon (Si), green (Cl), and orange (Cs).

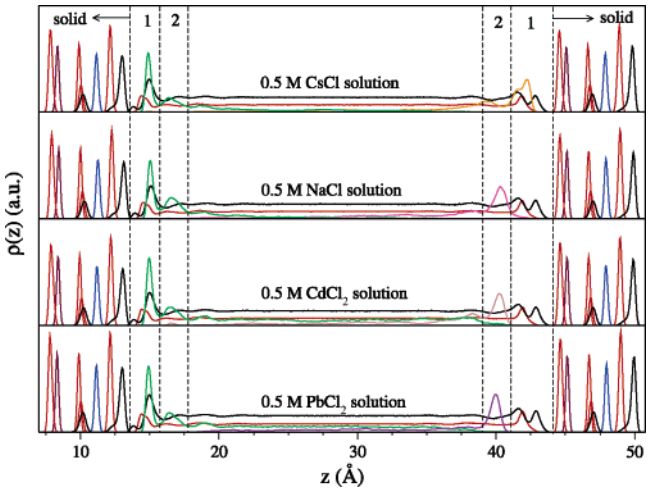

Figure 5. Atomic density profiles of the equilibrated 0.5 M solutions in contact with the two basal surfaces of kaolinite. Color key: red (O), black (H), blue (Al), maroon (Si), green (Cl), orange (Cs), magenta (Na), brown (Cd), and violet (Pb).

point they are randomly oriented as expected in bulk water.[27] This orientation of water molecules is not affected by the presence of ions in solutions.

The left-hand-side surface of Figure 4 represents the octahedral AlO_6 surface with the Al-bonded hydroxyls sticking out. The slightly positively charged surface attracts Cl^- ions. The reasonably narrow peak in the Cl^- density profile inside the inner-sphere region suggests a fairly strong interaction between Cl^- and the surface. This is confirmed by the distinct presence of a second and a third (for 0.5 and 1.0 M solutions) layer of Cl^- . The mechanism for Cl^- adsorption on this surface appears to be fairly concentration independent. Increasing height of peaks at inner- and outer-sphere distances with increasing concentration indicates a correlation between the number of anions apparently adsorbed and the number of anions present in solution. The long-lived presence of some Cs^+ inside the inner-sphere region for the 1.0 M case reinforces the Cl^- driven Cs^+ adsorption and ion pairing mechanism. Ion pairing is negligible for 0.5 M and nonexistent for 0.1 M.

At the opposite kaolinite surface, Si-bridging oxygen atoms relax outward slightly with respect to the silicon atoms and the surface has thus a very small net negative charge, which drives

TABLE 3: Adsorption Statistics Calculated from Atomic Density Profiles like Those in Figures 4 and 5

	Cl^-							Cs^+						
	inner sphere				total			inner sphere				total		
	N_{tot}	N_{ad}	X_{ad}	ρ	N_{ad}	X_{ad}	ρ	N_{tot}	N_{ad}	X_{ad}	ρ	N_{ad}	X_{ad}	ρ
0.1 M	7	3.4	49%	0.09	6.6	94%	0.18	7	4.7	66%	0.12	6.6	94%	0.18
0.5 M	32	10.8	34%	0.29	17.5	55%	0.47	32	12.9	40%	0.35	19.8	62%	0.53
1.0 M	64	14.7	23%	0.39	25.1	39%	0.67	64	14.3	22%	0.38	25.9	40%	0.69
	Cl^-							Na^+						
	inner sphere				total			inner sphere				total		
	N_{tot}	N_{ad}	X_{ad}	ρ	N_{ad}	X_{ad}	ρ	N_{tot}	N_{ad}	X_{ad}	ρ	N_{ad}	X_{ad}	ρ
0.1 M	7	3.5	50%	0.09	6.1	87%	0.16	7	0.3	4%	0.01	5.3	76%	0.14
0.5 M	32	10.7	33%	0.29	20.3	64%	0.54	32	0.9	3%	0.02	12.7	40%	0.34
1.0 M	64	18.8	29%	0.50	31.1	49%	0.83	64	0.7	1%	0.02	18.0	28%	0.48
	Cl^-							Cd^{2+}						
	inner sphere				total			inner sphere				total		
	N_{tot}	N_{ad}	X_{ad}	ρ	N_{ad}	X_{ad}	ρ	N_{tot}	N_{ad}	X_{ad}	ρ	N_{ad}	X_{ad}	ρ
0.1 M	14	6.1	44%	0.16	10.8	77%	0.29	7	0.0	0%	0.0	5.2	74%	0.14
0.5 M	64	12.7	20%	0.34	21.2	33%	0.57	32	0.0	0%	0.0	10.3	32%	0.28
1.0 M	128	18.3	14%	0.49	28.8	23%	0.77	64	0.0	0%	0.0	11.5	18%	0.31
	Cl^-							Pb^{2+}						
	inner sphere				total			inner sphere				total		
	N_{tot}	N_{ad}	X_{ad}	ρ	N_{ad}	X_{ad}	ρ	N_{tot}	N_{ad}	X_{ad}	ρ	N_{ad}	X_{ad}	ρ
0.1 M	14	5.8	42%	0.16	10.7	76%	0.28	7	0.0	0%	0.00	6.4	91%	0.17
0.5 M	64	12.9	20%	0.34	23.1	36%	0.62	32	0.0	0%	0.00	13.0	41%	0.35
1.0 M	128	17.0	13%	0.45	30.1	23%	0.80	64	0.0	0%	0.00	14.1	22%	0.38

Cs^+ ions toward it. The inner shell Cs^+ peak is significantly wider (it is actually a superposition of two very closely spaced peaks) than the Cl^- peak, which is a consequence of the large size and soft electron structure of Cs^+, in the sense that it does not usually bind strongly. At 0.1 M almost all the cations are found within the inner-sphere distance, as we suggested above, while at higher concentrations, some Cs^+ is also found in the outer-sphere region. Peaks consistent with inner-sphere Cs^+ at concentrations of 0.5 and 1.0 M are comparable in height with a little increase in the height of the more distant peak for the 1.0 M case, indicating that saturation is close to being achieved.

Figure 5 shows the atomic density profiles for 0.5 M CsCl, NaCl, $CdCl_2$, and $PbCl_2$ solutions in contact with kaolinite. Most of the Cd^{2+}, Pb^{2+}, and Na^+ ions are found at a distance to the surface consistent with outer-sphere adsorption, for the duration of the 500 ps period. The tail of the Na^+ peak leaks in the inner-sphere range suggesting some Na^+ inner-sphere adsorption, consistent with the inference made above based on the snapshot configurations.

To quantify the information inferred from the atomic density profiles like those in Figures 4 and 5, the various ion profiles are integrated over the inner-sphere and inner+outer-sphere regions to obtain the adsorption statistics shown in Table 3. The columns are as follows: N_{tot} is the total number of that particular ion in the system; N_{ad} is the number of ions within a particular region (inner sphere or total); X_{ad} is the percentage of the total number of ions N_{ad} represents; and ρ is the number of ions per unit surface area, in units of $1/nm^2$. ρ is equivalent to the adsorption site density.

Adsorption of Cl^- on the AlO_6 surface is affected by the type of cation present in solution. Cd^{2+} and Pb^{2+} seem to affect Cl^- adsorption in a similar way, resulting in consistent numbers in Table 3 for all three concentrations of $CdCl_2$ and $PbCl_2$. Numbers are also consistent for 0.1 M CsCl and NaCl solutions. However, for increasing ionic strengths, Cs^+ and Na^+ affect Cl^- adsorption in a different way. At 0.5 M, the amount of inner-sphere adsorption of Cl^- is virtually the same (ρ = 0.29 sites/nm^2) in the presence of both cations while outer-sphere adsorption is a little inhibited by the presence of Cs^+ (ρ = 0.18 sites/nm^2 as opposed to 0.26 sites/nm^2 in the presence of Na^+). At 1.0 M, both inner- and outer-sphere Cl^- adsorption is inhibited in the presence of Cs^+ (see table). This process is attributed to the formation of ion pairs close to the surface: a Cs^+ ion is significantly larger than a Na^+ ion (1.69 Å vs 0.95 Å) and tends to occupy space in which Cl^- ions would be found in a more significant way than Na^+ . This effect becomes more important with increasing number of ion pairs formed and with approach to saturation.

The valence of cations also seems to play a role on Cl^- adsorption. The loading of Cl^- on the surface for the same number of anions present in solution is consistently lower for divalent cations than it is for monovalent ones. This difference is attributed to the stronger interaction between Cl^- anions and divalent cations. Site densities are roughly 0.50 sites/nm^2 as inner sphere and 0.80 sites/nm^2 total at the highest load of Na^+ and both divalent cations, indicating that saturation of Cl^- on the AlO_6 surface is reached.

At the opposite kaolinite surface, inner-sphere site densities for Cs^+ are found to be 0.35 and 0.38 site/nm^2 for 0.5 and 1.0 M solutions, respectively, indicating saturation of Cs^+ adsorption sites on the surface. These numbers include the small Cl^--driven adsorption of Cs^+ on the AlO_6 surface, which accounts for just a negligible fraction of the total. In the same way, saturation densities are found to be 0.35−0.38 sites/nm^2 for Pb^{2+} and 0.30 sites/nm^2 for Cd^{2+}, revealing that Pb^{2+} has a slightly larger affinity to the surface than Cd^{2+}. As expected, no Cd^{2+} or Pb^{2+} is found within the inner-sphere range for this surface. It is also observed that less than 1 Na^+ is found at the inner-sphere distance regardless of the number of ions in

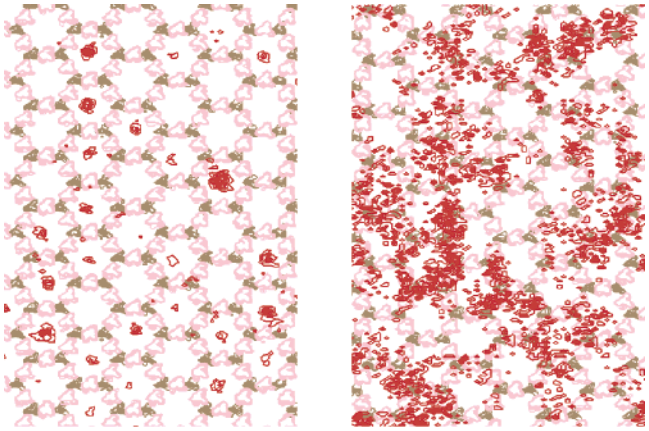

(a) inner sphere (1.0 M CsCl) (b) outer sphere (1.0 M CsCl)

Figure 6. Trajectory maps of Cs^+ within (a) inner- and (b) outer-sphere distances to the SiO_4 surface, superimposed to the trajectories of silicon and bridging oxygen atoms on the outmost layer of kaolinite. Obtained from the accumulated 500 ps of dynamics. A subset of the simulation cell is shown to better emphasize the details of the metal distributions. Color key: red (O), brown (Si), and orange (Cs^+).

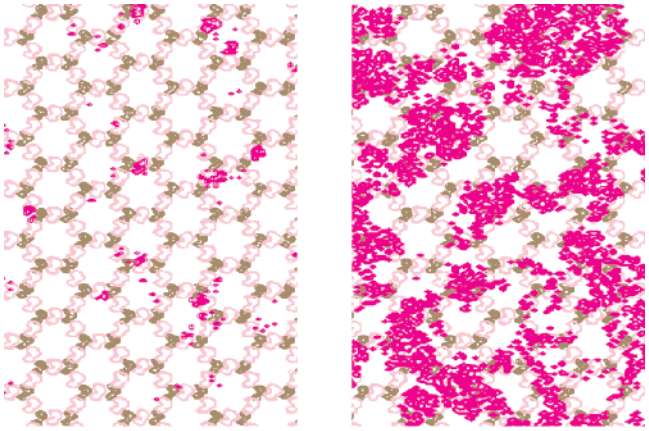

(a) inner sphere (1.0 M NaCl) (b) outer sphere (1.0 M NaCl)

Figure 7. Trajectory maps of Na^+ within (a) inner- and (b) outer-sphere distances to the SiO_4 surface, superimposed to the trajectories of silicon and bridging oxygen atoms on the outmost layer of kaolinite. Obtained from the accumulated 500 ps of dynamics. A subset of the simulation cell is shown to better emphasize the details of the metal distributions. Color key: red (O), brown (Si), and magenta (Na^+).

solution, and unlike Cs^+, a considerable fraction of this already small amount is due to adsorption on the AlO_6 surface.

3.2. Trajectory Maps. A trajectory map[27] is simply a map of the integrated atomic motions of chosen atomic types over the 500 ps of accumulated trajectories. Slices are selected along the *c* axis located at positions *i* and with thicknesses dz_i and map trajectories of the atoms onto a grid in the *a*−*b* plane. In our discussions, z_i and dz_i are always defined as the inner- and outer-sphere ranges described above at the solid−liquid interfaces.

Figure 6 shows the trajectories of Cs^+ ions within inner-sphere (a) and outer-sphere (b) ranges from the SiO_4 surface, superimposed on the trajectories of silicon and bridging oxygen atoms on the outermost layer of kaolinite. The trajectories indicate that inner-sphere Cs^+ ions are found preferentially over the hexagonal cavities on the surface, and have little mobility beyond the center of the cavity. Outer-sphere trajectories, on the other hand, are quite diffuse over the whole surface with little indication of long-lived complex formation.

Unlike Cs^+ ions within inner-sphere distances from the SiO_4 surface, the Na^+ adsorption site is asymmetrical with respect to the hexagonal rings (offset in comparison to the symmetrical Cs^+ site), as can be seen in Figure 7a, and this is the result of the smaller ionic radius of Na^+ and the local kaolinite charge as affected by the octahedral vacancy. Outer-sphere Na^+ ions, like Cs^+ in the same situation, are quite mobile on the *a*−*b* plane with no formation of stable long-lived complexes (see Figure 7b).

Figure 8 shows trajectory maps of (a) Cd^{2+} and (b) Pb^{2+} ions within outer-sphere distances from the SiO_4 surface. It has been seen above that these ions are not found inside the inner-sphere region for this surface. It is clear from the trajectory maps that both Cd^{2+} and Pb^{2+} cations are mostly found on the hexagonal cavities on the surface, just like the inner-sphere Cs^+ ions. The trajectories are not so tightly concentrated around the centers of the cavities as the inner-sphere Cs^+ ones, indicating that these complexes are not quite as stable, which is not surprising considering the longer distance and the presence of water molecules between the cations and the surface.

Figure 9 shows the trajectories for 1.0 M CsCl solution in contact with the AlO_6 surface. Cl^- anions clearly adsorb as inner-sphere complexes above the aluminum vacancy and are coordinated by three oriented hydroxyls. Inner-sphere Cs^+

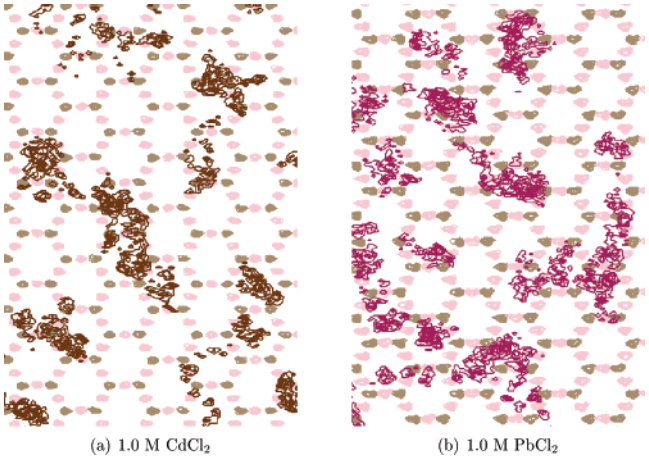

(a) 1.0 M $CdCl_2$ (b) 1.0 M $PbCl_2$

Figure 8. Trajectory maps of (a) Cd^{2+} and (b) Pb^{2+} within the outer-sphere distance to the SiO_4 surface, superimposed to the trajectories of silicon and bridging oxygen atoms on the outmost layer of kaolinite. Obtained from the accumulated 500 ps of dynamics. A subset of the simulation cell is shown to better emphasize the details of the metal distributions. Color key: red (O), brown (Si), maroon (Cd^{2+}), and violet (Pb^{2+}).

complexes also occur, almost always coordinated as an ion pair with Cl^-. Na^+-Cl^- pair formation also occurs while $Pb^{2+}-Cl^-$ and $Cd^{2+}-Cl^-$ pairs do not (not shown). Outer-sphere Cl^- trajectories are more diffuse indicating weaker adsorption, as expected for outer-sphere complexes.

3.3. Radial Distribution Functions and Structural Information about Adsorption Sites. Before proceeding with further discussion of these results, it is advisable to summarize the findings so far. On the AlO_6 octahedral surface, strong Cl^- inner-sphere adsorption is found above aluminum vacancies and weak outer-sphere adsorption. Formation of inner-sphere Cs^+-Cl^- and Na^+-Cl^- complexes is also identified. Cl^--controlled adsorption of Cd^{2+} and Pb^{2+} does not occur.

Regarding the SiO_4 tetrahedral surface, a fairly strong adsorption of Cs^+ as inner sphere associated with the hexagonal cavities could be identified. Despite the presence of a peak in the Cs^+ density profile consistent with outer-sphere adsorption, the diffuse trajectories indicate very weak adsorption. Similar reasoning applies to outer-sphere Na^+ ions. Inner-sphere Na^+ complex formation also occurs although not necessarily at a

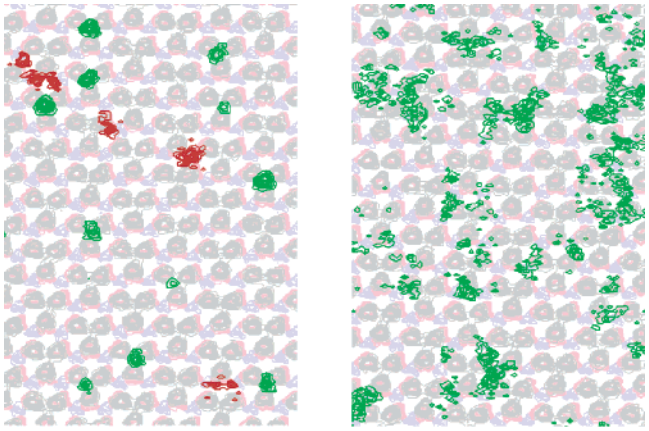

Figure 9. Trajectory maps of the 1.0 M CsCl solution in equilibrium with the AlO_6 kaolinite surface within (a) inner- and (b) outer-sphere ranges. Obtained from the accumulated 500 ps of dynamics. A subset of the simulation cell is shown to better emphasize the details of the ion distributions. Color key: red (O), gray (H), blue (Al), green (Cl^-), and orange (Cs^+).

fixed site. No Cd^{2+} and Pb^{2+} are found inside the inner-sphere region. However, fairly stable and long-lived outer-sphere Cd^{2+} and Pb^{2+} complexes exist, confirmed by both atomic density profile and trajectory maps. Like inner-sphere Cs^+ complexes, outer-sphere Cd^{2+} and Pb^{2+} complexes adsorb at the hexagonal cavity.

Table 4 shows values of solvation and inner-sphere adsorption (on the SiO_4 surface) energies for the various cations. The solvation energy is the energy associated with a fully hydrated ion and is calculated as the energy difference between the solvated ion and that of the solvent. The inner-sphere adsorption energy is defined here as the energy associated with an inner-sphere adsorption complex and is calculated by taking the energy difference between a solution−mineral system with a cation adsorbed at a surface hexagonal cavity as an inner-sphere complex and that of the same system without the cation present.

The solvation energy is a measure of the energetic penalty associated with separating an ion from its hydration shell, while the inner-sphere adsorption energy is the energy it takes to remove from the system an ion that is sorbed at a hexagonal cavity. Comparing these two energies for the same type of ion gives us a measure of how energetically favorable/unfavorable it is to take an ion from the bulk solution and form an inner-sphere adsorption complex, and vice versa.

Because Cs^+ has a very large ionic size and charge of just +1, the water molecules of its hydration shell are not very tightly bound. There is a fairly large amount of water molecule exchange between the hydration shell and the bulk solution. As a consequence, the solvation and inner-sphere adsorption energies of Cs^+ in Table 3 are such that it is energetically favorable for Cs^+ to lose part of its hydration sphere and adsorb directly to the surface as an inner-sphere complex, despite its weak interaction with the surface.

Na^+ ions are considerably smaller than Cs^+ ions and so have a slightly larger (more negative) solvation energy than Cs^+ (see Table 3) and therefore the water molecules are more strongly bound to Na^+ than to Cs^+ . The solvation energy of Na^+ is just a little more negative than its inner-sphere adsorption energy (see Table 4) indicating that it is not so favorable for Na^+ to adsorb directly to the surface at the expense of fewer water molecules on its hydration shell. However, the energy difference does allow for a few Na^+ ions to get close to the surface.

Cd^{2+} and Pb^{2+} have, in turn, a charge of +2 and interact more strongly with the water molecules, keeping them tightly bound on a fairly stable hydration shell. It is very costly energetically to remove water molecules from the hydration shells of the cations and as a consequence, no Cd^{2+} or Pb^{2+} can be found inside the inner-sphere regions. The electrostatic interaction between the divalent Cd^{2+} and Pb^{2+} is still strong enough to keep the hydrated cation adsorbed as outer-sphere complexes. Such interaction is not strong enough for the monovalent Cs^+ and Na^+ to form stable outer-sphere adsorption complexes, and that explains the diffuse trajectories.

Radial distribution functions (RDF)[42] are used to characterize the structure of adsorption sites on the SiO_4 surface. An RDF, $g_{ij}(r)$, is the simplest one of a set of correlation functions between particles. It translates the probability, averaged over time, of finding a pair of atoms of types i and j separated by a distance between r and $r + \delta r$ (δr is a small number), with respect to the probability expected from a completely random distribution of particles with the same density. The existence of a coordinated shell of atoms of type j at a certain distance around atoms of type i is manifested by the presence of a peak in the RDF centered at a position corresponding to this distance. The average

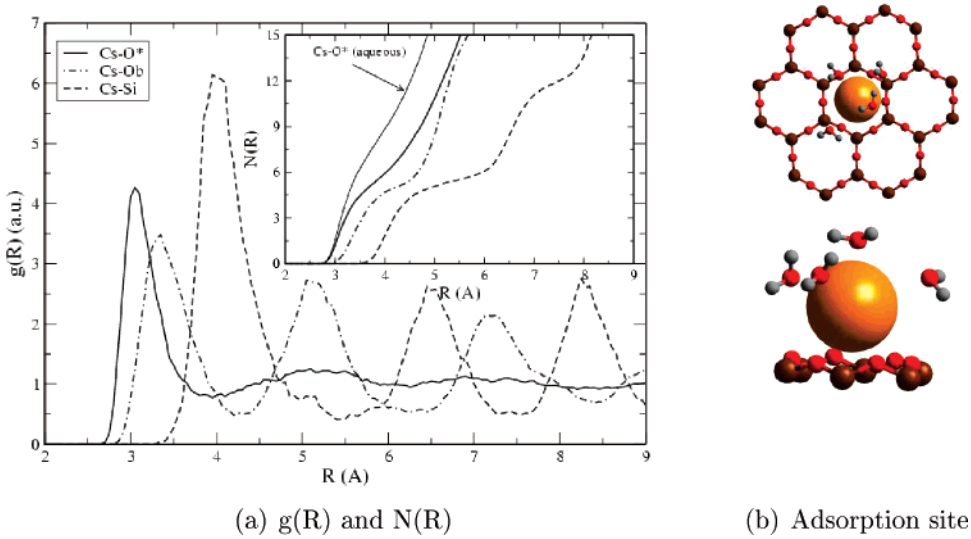

Figure 10. (a) Radial distribution functions and coordination numbers (detail) for a 0.1 M CsCl solution in equilibrium with kaolinite. (b) Graphical representation of a typical Cs^+ adsorption complex.

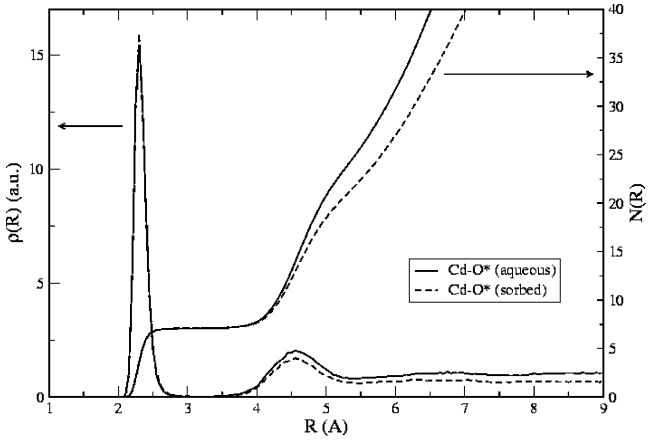

Figure 11. Radial distribution functions and coordination numbers calculated from a 0.1 M $CdCl_2$ bulk solution and from a 0.1 M $CdCl_2$ solution in equilibrium with kaolinite.

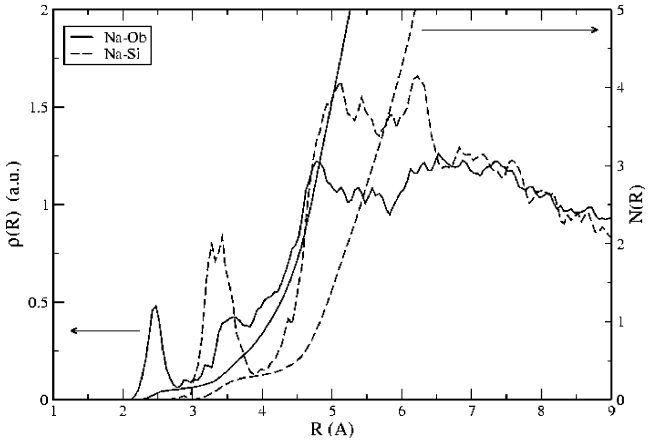

Figure 13. Radial distribution functions and coordination numbers for a 0.1 M NaCl solution in equilibrium with kaolinite.

TABLE 4: Solvation and Inner-Sphere Adsorption Energies for the Various Cations on the Siloxane Surface of Kaolinite[a]

	energies (kcal/mol)	
ion	solvation	adsorption
Cs^+	−59	−74
Na^+	−89	−69
Cd^{2+}	−370	−100
Pb^{2+}	−313	−99

[a] Uncertainties are ∼4 kcal/mol for all values.

number of atoms in this shell is given by the area under the peak and is obtained by integrating $g_{ij}(r)$ from immediately before to immediately after the peak. Typically, the positions at the minima of the curve that precede and follow it are chosen as the limits of this peak, or just a point where the RDF is zero when this is the case.

Figure 10a shows RDFs with Cs^+ ions in the central position calculated from an equilibrated 0.1 M CsCl solution in contact with kaolinite averaged over 500 ps. Only inner-sphere cations are included in the calculations. Cs−O*, Cs−Ob, and Cs−Si RDFs correspond to the configuration of water oxygen (O*), bridging oxygen (Ob), and silicon (Si) atoms, respectively, around the aforementioned Cs^+ ions. The graph in the detail shows the average number of atoms of these three species as a function of distance to the central cation, along with the Cs−O* number of atoms curve calculated from Cs^+ solvated in bulk water. A graphical representation of a typical adsorption complex on the *a*−*b* plane (top) and along the *c* axis (bottom) is shown in Figure 10b.

The Cs−O* RDF presents a pronounced peak corresponding to a first hydration shell, and a diffuse peak for the second shell. The absence of a clear separation between first and second hydration shells is a consequence of the weak interaction between Cs^+ and water molecules mentioned above. This peak is defined between 2 Å and roughly 3.9 Å and is centered at ∼3.12 Å. The uncertainty in this distance is estimated as the half-width at half-height of the peak and is ∼0.25 Å. The number of water molecules in the first hydration shell is obtained from the corresponding $N(R)$ curve at a distance $R \approx 3.9$ Å. The coordination number of the first hydration shell of Cs^+ decreases from 8.3 for the solvated ion to 5.6 for the adsorbed ion. The distance of 3.12 Å remains unchanged. All distances, coordination numbers, and uncertainties given in the following are obtained in this same fashion.

Cs−Ob and Cs−Si RDFs, on the other hand, have several peaks up to large distances as expected from the crystal structure of the substrate. The first peak in each of the Cs−Ob and Cs−Si RDFs corresponds to 5.1 Ob atoms and 5.4 Si atoms 3.42 and 4.06 Å distant from the Cs^+ ion. This picture is consistent with inner-sphere adsorption on a cavity formed by the Ob and

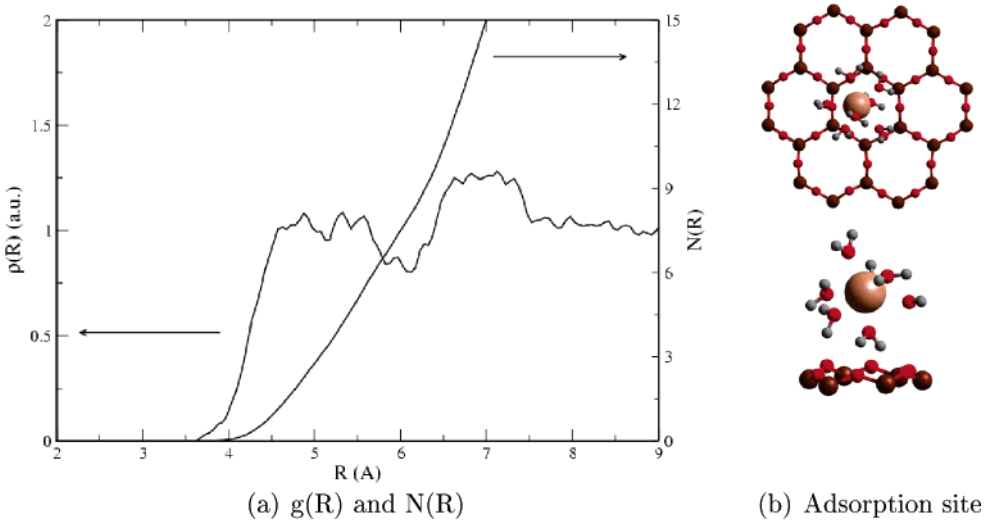

Figure 12. (a) Cd−Ob radial distribution function and coordination number calculated from a 0.1 M $CdCl_2$ solution in equilibrium with kaolinite. (b) Graphical representation of a typical Cd^{2+} adsorption complex.

TABLE 5: Coordination Numbers (*N*) and Characteristic Distances (*R*) of Aqueous and Sorbed Complexes

	N			*R* (Å)		
shell	this work	exptl[f]	other MM[g]	this work	exptl[f]	other MM[g]
aqueous Cs^+						
Cs−O* first	8.1 (0.8)	6−8[a]	5.3−8.2[a]	3.12 (0.25)	2.95−3.21[a]	3.03−3.20[a]
sorbed Cs^+ (inner sphere)						
Cs−O* first	5.4 (0.6)			3.12 (0.25)		
Cs−Ob	5.1 (0.4)			3.41 (0.31)		
Cs−Si	5.4 (0.4)			4.06 (0.34)		
aqueous Na^+						
Na−O* first	5.5 (0.3)	4−8[a]	6[a]	2.37 (0.15)	2.40−2.50[a]	2.30−2.40[a]
Na−O* second	16.7 (3.0)		12.4[a]	4.47 (0.57)		4.41−4.80[a]
aqueous Cd^{2+}						
Cd−O* first	7.0 (0.2)	6[b]	6[c]	2.31 (0.11)	2.27−2.31[b]	3.33−3.35[c]
Cd−O* second	16.6 (2.0)	12[a]	11.7−12.2[c]	4.59 (0.38)	4.31−4.37[a]	4.8−4.9[c]
sorbed Cd^{2+} (outer sphere)						
Cd−O* first	7.0 (0.2)			2.31 (0.11)		
Cd−O* second	13.4 (2.0)			4.57 (0.38)		
Cd−Ob	6.5			5.10		
aqueous Pb^{2+}						
Pb−O* first	8.4 (0.2)	6−11[d]	8−9[e]	2.65 (0.13)	2.45−2.60[d]	2.60−2.65[e]
Pb−O* second	20.9 (2.0)		24[e]	4.90 (0.40)		5.0[e]
sorbed Pb^{2+} (outer sphere)						
Pb−O* first	8.4 (0.2)			2.65 (0.13)		
Pb−O* second	18.1 (2.0)			4.89 (0.42)		
Pb−Ob	6.5			5.40		

[a] Reference 43. [b] References 44 and 43. [c] Reference 45. [d] Reference 46. [e] Reference 47. [f] Experimental results. [g] Other molecular modeling simulations.

Si hexagonal lattices rotated by 30° with respect to each other (Figure 10b).

Figure 11 shows aqueous and sorbed Cd−O* RDFs along with the average number of atoms as a function of distance to the central atom. Pb^{2+} $g(R)$ and $N(R)$ are not shown but the behavior is very similar to that of Cd^{2+} and the analysis follows in the same way. Cations in the bulk solution are left out of the adsorbed Cd−O* and Pb−O* calculations to ensure that the structure of outer-sphere adsorption complexes is isolated. Bulk solution and adsorbed Cd−O* and Pb−O* (not shown) RDFs present the same first shell of oxygen atoms with the same coordination numbers of 7.0 and 8.4 and distances of 2.31 and 2.65 Å for Cd^{2+} and Pb^{2+}, respectively. This indicates that the first hydration shell remains unchanged. The presence of the surface makes the second hydration shells of adsorbed complexes have about 2.5 to 3 fewer water molecules, on average, than aqueous complexes. Cd−Ob (Figure 12a) and Pb−Ob (not shown) RDFs are very diffuse without a sharp separation between the first shell and the remaining Ob atoms in the substrate crystal. Nevertheless, the presence of a defined shell centered at about 5.1 Å for Cd^{2+} and 5.4 Å for Pb^{2+} with 5−7 atoms in it can be clearly identified. This description is consistent with a fully hydrated Cd^{2+} ion adsorbed on a hexagonal cavity on the surface.

The hydration shells of Na^+ in the bulk water and within adsorption distance from the surface follow very closely the ones of Cd^{2+} and Pb^{2+}. The first shell is virtually unchanged while the second shell loses about three water molecules (not shown). The coordination of Na^+ with the surface, however, does not follow that of Cd^{2+} and Pb^{2+}, as can be seen in the Na−Ob and Na−Si in Figure 13. The sharp peaks between 2 and 4 Å correspond to the few Na^+ ions found within the inner-sphere range as pointed out previously. Coordination numbers of less than 1 are consistent with Na^+ staying directly above either a Si or an Ob atom rather than the hexagonal cavity. Moreover, the absence of clear coordination shells beyond those just mentioned in either Na−Ob or Na−Si confirms the suggestion of high mobility of Na^+ ions within the outer-sphere distance and the absence of strongly bound adsorption sites.

Table 5 summarizes all the structural parameters for aqueous and adsorbed complexes calculated from RDFs along with reference numbers obtained from the literature. Our parameters for the hydration shell of aqueous Cs^+ are in very good agreement with those obtained from experiments and other simulations. So are the parameters for the Pb^{2+} first hydration shell. Cd−O* distances for both the first and second hydration shells are in good agreement with experimental results, while the coordination numbers are in slight disagreement. A first shell coordination number of 7 is found, while it is consistently reported as 6. The second shell coordination number found is more than 2 units lower than what is reported, even after accounting for the uncertainty of our calculations. Coordination numbers and distance for aqueous Na−O* are in reasonable agreement with results from both experiments and other molecular modeling simulations.

4. Conclusions

Molecular dynamics simulations were used to study the interaction between aqueous ions and the basal surfaces of kaolinite. The pair interaction between atoms in the system was modeled by using the CLAYFF force field. CLAYFF is very robust (the only bonded interactions are within water molecules and hydroxyls) and successfully models mineral/aqueous solution interfaces, as confirmed in this study.

Kaolinite and its interface with aqueous solutions of CsCl, NaCl, $CdCl_2$, and $PbCl_2$ at concentrations of 0.1, 0.5, and 1.0 M was studied. Analysis of simulation data indicates that cations and anions adsorb preferably on the siloxane and gibbsite surfaces of kaolinite, respectively. Strong inner-sphere adsorption of chlorine at aluminum vacancies on the gibbsite surface and the occurrence of chlorine-driven inner-sphere adsorption of cesium and sodium on the gibbsite surface for high ionic strengths was found. Cesium ions form strong inner-sphere complexes at ditrigonal cavities on the siloxane surface. Outer-sphere cesium is highly mobile and only weak adsorption may occur. A small amount of sodium adsorbs on the siloxane surface as inner-sphere complexes at not clearly defined sites. Like

cesium, sodium only forms very weak outer-sphere complexes on this surface. Inner-sphere complexes of cadmium and lead do not occur on either surface. Relatively strong outer-sphere cadmium and lead complexes are present on the siloxane surface at ditrigonal cavities. Calculated solvation and inner-sphere adsorption (on the siloxane surface) energies for the various cations help explain the behavior of adsorbed ions on this surface. Structural parameters such as coordination numbers and characteristic distances obtained from radial distribution functions are mostly in agreement with experimental and molecular modeling results published in the literature.

Acknowledgment. We thank the U.S. Department of Energy, Office of Basic Energy Sciences for funding to RTC through the Environmental Molecular Science Institute program. Sandia is a multiprogram laboratory operated by Sandia Corporation, a Lockheed Martin Company for the United States Department of Energy's National Nuclear Security Administration under contract DE-AC04-94AL85000. We also thank Dr. A. Kalinichev for help with the trajectory analysis software and Dr. J. C. Ducom for the help with the parallel Linux cluster housed at the University of Notre Dame.

References and Notes

(1) Brady, P. V.; Cygan, R. T.; Nagy, K. L *J. Colloid. Interface Sci.* **1996**, *183*, 356.
(2) Huertas, F. J.; Chou, L.; Wollast, R. *Geochim. Cosmochim. Acta* **1998**, *62*, 417.
(3) Sutheimer, S. H.; Maurice, P. A.; Zhou, Q. H. *Am. Mineral.* **1999**, *84*, 620.
(4) Ganor, J.; Cama, J.; Metz, V. *J. Colloid. Interface Sci.* **2003**, *264*, 67.
(5) Cygan, R. T.; Liang, J. J.; Kalinichev, A. G. *J. Phys. Chem. B* **2004**, *108*, 1255.
(6) Kim, Y.; Cygan, R. T.; Kirkpatrick, R. J. *Geochim. Cosmochim. Acta* **1996**, *60*, 1041.
(7) Sposito, G. *Rev. Mineral.* **1990**, *23*, 261.
(8) Spark, K. M.; Wells, J. D.; Johnson, B. B. *Eur. J. Soil Sci.* **1995**, *46*, 633.
(9) Forbes, E. A.; Posner, A. M.; Quirk, J. P. *J. Soil Sci.* **1976**, *27*, 154.
(10) Schindler, P. W.; Liechti, P.; Westall, J. C. *Neth. J. Agric. Sci.* **1987**, *35*, 219.
(11) Angove, M. J.; Johnson, B. B.; Wells, J. D. *Colloids Surf., A* **1997**, *126*, 137.
(12) Angove, M. J.; Johnson, B. B.; Wells, J. D. *J. Colloid. Interface Sci.* **1998**, *204*, 93.
(13) Echeverria, J. C.; Churio, E.; Garrido, J. J. *Clays Clay Miner.* **2002**, *50*, 614.
(14) Reed, B. E.; Carriere, P. C.; Moore, R. *J. Environ. Eng.* **1996**, *122*, 48.
(15) Ikhsan, J.; Johnson, B. B.; Wells, J. D. *J. Colloid. Interface Sci.* **1999**, *217*, 403.
(16) Strawn, D. G.; Sparks, D. L. *J. Colloid. Interface Sci.* **1999**, *216*, 257.
(17) Hepinstall, S. E.; Turner, B. F.; Maurice, P. A. *Clays Clay Miner.* **2005**, *53*, 557.
(18) Komarneni, S. *Soil Sci. Soc. Am. J.* **1978**, *42*, 531.
(19) Evans, D. W.; Albers, J. J.; Clark, R. A., III *Geochim. Cosmochim. Acta* **1983**, *47*, 1041.
(20) Westrich, H. R.; Cygan, R. T.; Brady, P. V.; Nagy, K. L.; Anderson, H. L.; Kim, Y.; Fitzpatrick, R. J. The Sorption Behavior of Cs and Cd onto Oxide and Clay Surfaces. In *Proceedings of the waste management conference, WM'95*.
(21) Kim, Y.; Kirkpatrick, R. J.; Cygan, R. T. *Geochim. Cosmochim. Acta* **1996**, *60*, 4059.
(22) Kemner, K. M.; Hunter, D. B.; Bertsch, P. M.; Kirkland, J. P.; Elam, W. T. *J. Phys. IV* **1997**, *7*, 777.
(23) McKinley, J. P.; Zachara, J. M.; Heald, S. M.; Dohnalkova, A.; Newville, M. G.; Sutton, S. R. *Environ. Sci. Technol.* **2004**, *38*, 1017.
(24) Bostick, B. C.; Vairavamurthy, M. A.; Karthikeyan, K. G.; Chorover, J. *Environ. Sci. Technol.* **2002**, *36*, 2670.
(25) Zachara, J. M.; Smith, S. C.; Liu, C. X.; McKinley, J. P.; Serne, R. J.; Gassman, P. L. *Geochim. Cosmochim. Acta* **2002**, *66*, 193.
(26) Nakano, M.; Kawamura, K.; Ichikawa, Y. *Appl. Clay Sci.* **2003**, *23*, 15.
(27) Wang, J.; Kalinichev, A. G.; Kirkpatrick, R. J.; Cygan, R. T. *J. Phys. Chem. B* **2005**, *109*, 15893.
(28) Greathouse, J. A.; Cygan, R. T. *Phys. Chem. Chem. Phys.* **2005**, *7*, 3580.
(29) Payne, M. C.; Teter, M. P.; Allan, D. C.; Arias, T. A.; Joanopoulos. J. D. *Rev. Mod. Phys.* **1992**, *64*, 1045.
(30) Berendsen, H. J. C.; Postma, J. P. M; van Gunsteren, W. F.; Hermans, J. Interaction models for water in relation to protein hydration. In *Intermolecular Forces*; Pullman, B., Ed.; D. Reidel: Amsterdam, The Netherlands, 1981; p 331.
(31) Teleman, O.; Jonsson, B.; Engstrom, S. *Mol. Phys.* **1987**, *60*, 193.
(32) Wallqvist, A.; O Teleman, O. *Mol. Phys.* **1991**, *74*, 515.
(33) Smith, D. E.; Haymet, A. D. J. *Fluid Phase Equilib.* **1993**, *88*, 79.
(34) Plimpton, S. *J. Comput. Phys.* **1995**, *117*, 1.
(35) Hoover, W. G. *Phys. Rev. A* **1986**, *34*, 2499.
(36) Martyna, G. J.; Tobias, D. J.; Klein, M. L. *J. Chem. Phys.* **1994**, *101*, 4177.
(37) Nosé, S. *Mol. Phys.* **1984**, *52*, 255.
(38) Hoover, W. G. *Phys. Rev. A* **1985**, *31*, 1695.
(39) Verlet, L. *Phys. Rev.* **1967**, *159*, 98.
(40) Verlet, L. *Phys. Rev.* **1968**, *165*, 201.
(41) Ewald, P. *Ann. Phys.* **1921**, *64*, 253.
(42) Rahman, A. *Phys. Rev.* **1964**, *136*, A405.
(43) Ohtaki, H.; Radnai, T. *Chem. Rev.* **1993**, *93*, 1157.
(44) Boyanov, M. I.; Kelly, S. D.; Kemner, K. M.; Bunker, B. A.; Fein, J. B.; Fowle, D. A. *Geochim. Cosmochim. Acta* **2003**, *67*, 3299.
(45) Kritayakornupong, C.; Plankensteiner, K.; Rode, B. M. *J. Phys. Chem. A* **2003**, *107*, 10330.
(46) Mishra, B.; Haack, E. A.; Maurice, P. A.; Bunker, B. A. *Environ. Sci. Technol.* In preparation.
(47) Hofer, T. S.; Rode, B. M. *J. Chem. Phys.* **2004**, *121*, 6406.